UNIVERSIDAD DE CONCEPCIÓN
FACULTAD DE CIENCIAS FÍSICAS Y MATEMÁTICAS
MAGÍSTER EN ASTRONOMÍA

Molecular gas properties of Q1700-MD94: a massive, main-sequence galaxy at $z \approx 2$

Propiedades del gas molecular de Q1700-MD94: Una galaxia masiva y de sequencia principal a $z \approx 2$

Autor:
Katherine Henríquez-Brocal

Profesor Guía:
Prof. Rodrigo Herrera-Camus

Comisión:
Rodrigo Herrera-Camus, Ricardo Demarco, Stefano Bovino.

Tesis para ser presentada a la Dirección de Postgrado de la Universidad de Concepción para optar al grado académico de Magíster en Astronomía

CONCEPCIÓN, CHILE
2021

Molecular gas properties of Q1700-MD94: a massive, main-sequence galaxy at $z \approx 2$

Abstract

We use a combination of new NOrthern Extended Millimeter Array (NOEMA) observations of the pair of [CI] transitions, the CO(7-6) line, and the dust continuum, in addition to ancillary CO(1-0) and CO(3-2) data, to study the molecular gas properties of Q1700-MD94, a massive, main-sequence galaxy at $z \approx 2$. We find that for a reasonable set of assumptions for a typical massive star-forming galaxy, the CO(1-0), the [CI](1-0) and the dust continuum yield molecular gas masses that are consistent within a factor of ~ 2. The global excitation properties of the molecular gas as traced by the [CI] and CO transitions are similar to those observed in other massive, star-forming galaxies at $z \sim 2$. Our large velocity gradient (LVG) modeling using RADEX of the CO and [CI] spectral line energy distributions (SLEDs) suggests the presence of low-excitation ($T_{\rm kin} = 34$ K, $n_{\rm H_2} = 3.1 \times 10^3$ cm^{-3}) and high-excitation ($T_{\rm kin} = 137$ K, $n_{\rm H_2} = 1.6 \times 10^4$ cm^{-3}) molecular gas components. While the former is responsible for the bulk of the [CI](1-0) and [CI](2-1) line emission, the later dominates the CO line emission at $J \gtrsim 4$. The galaxy size in the CO(1-0) and CO(7-6) line emission are comparable, which suggests that the highly-excited molecular gas is distributed throughout the disk powered by intense star formation activity. To confirm this scenario will require spatially resolved observations of the CO and [CI] lines which can now be obtained with NOEMA upgraded capabilities.

Acknowledgements

Quiero agradecer a todos los que hicieron posible mi magíster y el desarrollo de mi tesis:
- A mi familia quienes me apoyaron en esta etapa de mi vida, especialmente a mi madre Allinka Brocal Winkler a quien le debo todos mis logros. Agradecer a mi novio Marco Albán Morales quien ha estado a mi lado en todo el proceso y más, siempre apoyándome y ayudándome en lo que yo necesite. - Al profesor Rodrigo Herrera-Camus, mi asesor de tesis, quien no solo me enseñó y guió por este camino de la investigación, sino que también me inspiró para querer ser mejor científico. El apoyo del grupo Max planck del cual somos parte también fue clave en este proceso. - Mis profesores y compañeros de la Universidad de Concepción quienes dedicaron su tiempo y paciencia para enseñarme lo que ellos saben. - Al grupo de investigación Galssev, especialmente al profesor Ricardo Demarco quien me incluyó en su grupo y me apoyó desde el primer día de magíster. - A mi equipo de divulgación astronómica (EDA) y extensión, por dejarme ser el canal de transmisión entre la ciencia y el público general. - Agradecer a todos mis amigos que siempre me desearon lo mejor. - Y por último, agradecerme a mí, por nunca rendirme.

K.H.B. and R.H.-C. thanks the Max Planck Society for support under the Partner Group project "The Baryon Cycle in Galaxies" between the Max Planck for Extraterrestrial Physics and the Universidad de Concepción. K.H.B. and R.H.-C. also would like to thank C. Lefèvre, C. Herrera and the rest of the IRAM staff for their help with the data calibration. This work is based on observations carried out under project number W17DL with the IRAM NOEMA Interferometer. IRAM is supported by INSU/CNRS (France), MPG (Germany) and IGN (Spain). R.H.-C. and R.D. gratefully acknowledges support from the Chilean Centro de Excelencia en Astrofísica y Tecnologías Afines (CATA) BASAL grant AFB-170002. M.R. acknowledge support from ANID (Chile) Fondecyt grant No 1190684.

Contents

List of Figures

List of Tables

Chapter 1

Introduction

To understand this work, it is necessary to know a key element of the evolution of galaxies: the interstellar medium (ISM). The ISM is the gas and dust that lies between stars, with Hydrogen gas being the main protagonist at 70%, then He at 28% and other heavier elements at 2% (e.g., Ferrière, 2001). Despite the fact that the ISM only represents 0.5% of the total mass of the galaxy (Dyson and Williams, 1997), multiple physical processes of micro and macro scale take place in it, which allows us to elucidate where and when the stars will form.

The ISM is widely distributed throughout the galaxy, but mainly confined to the disk and is very faint. Because He is present in low quantity and has a low degree of chemical reactivity, that is, it has little propensity to form molecules and compounds, the gas is categorized according to Hydrogen gas, which can be found in different phases depending on of its density and temperature conditions: molecular (H_2), atomic (HI) and ionized (HII), with a wide range of temperatures ($10 - 10^6$ K) and densities ($10^{-3} - 10^6$ cm^{-3}) (e.g., Tielens, 2005). We can find all these phases coexisting in the ISM, organizing themselves in orderly structures such as clouds and clumps, depending on the environmental conditions.

HII is typically found at the edges of the cloud because the gas in this area is closer to ionizing radiation from OB spectral stars, and other events such as supernova explosions (SNe) (e.g., Draine, 2011). The HI regions are found between the ionized and molecular gas phases. In general, the 21 cm line is used to study the atomic regions, since its emission is concentrated in the superfine transition of Hydrogen at 1420 MHz. Further inside the cloud, in the densest zones, we can find the H_2 clouds. This is where the ideal conditions to form stars meet and is thought to be the phase immediately preceding star formation (e.g., Leroy et al., 2008). The H_2 gas manages to remain non-ionized and suitable to form stars. Due to its high density, this molecule is able to protect itself from UV photodissociation due to dust shielding and its own self-shielding (e.g., Lequeux, 2005; Tielens, 2005)

Photodissociation regions (PDR) are another important part of the ISM. They are a transition zone between ionized and molecular gas. It is in these regions where the photons in the far-ultraviolet (FUV), produced by massive stars, heat up the gas via the photoelectric effect on dust grains. A schematic of a typical PDR region is shown in Fig. 1.1. From left to right, extinction increases and molecules like H_2 can coexist with others since they are more protected due to dust.

H_2 does not present a net dipole moment, that is, it does not have rotational lines, making it impossible to observe in the radio wavelength. Fortunately, clouds contain more elements

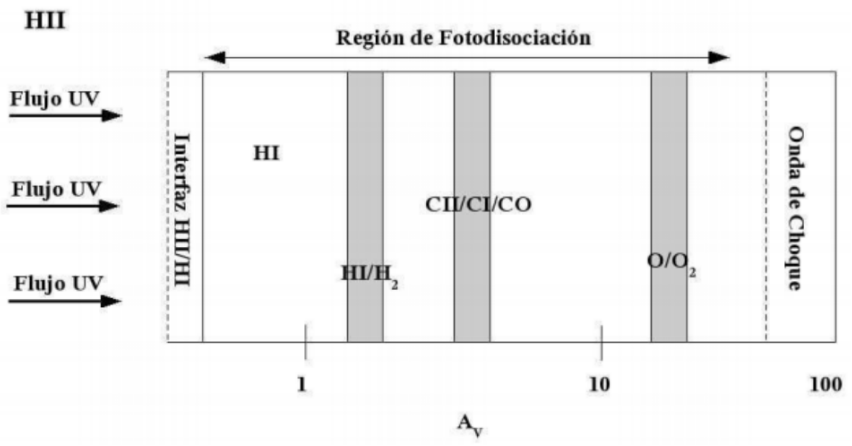

FIGURE 1.1. Typical diagram of a photodissociation region within a cloud. UV radiation comes from massive O-B like stars producing a first layer of HII. Further inside, with a greater extinction and more protected from radiation, are the H2 regions where new stars will be able to form. Image: Hollenbach and Tielens (1997)

in addition to Hydrogen, which is why the second most abundant molecule in molecular clouds is used, carbon monoxide (CO). Because the required temperature for CO in its first excited state is only ∼5 K, it is easy for it to get excited, even in cold clouds (Carilli and Walter, 2013), making the CO emission line (J = 1-0) a good tracer of molecular gas.

Since our interest is based on measuring the amount of molecular gas and not CO, we must do it indirectly through the luminosity of CO and transform it to obtain the mass of molecular gas. We use a conversion factor apha$_{co}$ (e.g., Bolatto et al., 2013) that will be discussed later in the text. Determining the $\alpha_{\rm CO}$ is not easy, it depends on the metallicity of the cloud, among other things. The enrichment will be greater once the stars end their life and the elements that were fused inside them are returned to the ISM. This will make the gas clouds richer in metals.

Molecular clouds at high redshift can show little extinction due to its low metallicity (see Fig. 1.2), which makes the gas more exposed to radiation and the observation of CO more difficult due to the photodissociation of this molecule (Bolatto et al., 2013). Due to these uncertainties, the need arises for another tracer, and atomic carbon ([CI]) has gained popularity. The advantage of using [CI] as a molecular gas tracer is that the excitation temperature can be determined directly, only using the transitions [CI] (1-0) at 492.161 GHz and [CI] (2-1) at 809.344 GHz (Stutzki et al., 1997).

Authors such as Valentino et al. (2018, 2020b) have studied high redshift systems, finding that the [CI](1-0) transition is a good tracer of the molecular gas mass, similar to low-J CO lines and dust. They also find that the gas temperature traced by the [CI] lines do not strongly vary across galaxy types and redshift. Furthermore, this study supports the coexistence between CO and [CI] because the most extreme relationships for the line ratio of [CI] are similar to the mean relationships of CO ($L'_{\rm CO(7-6)}/L'_{\rm CO(1-0)}$).

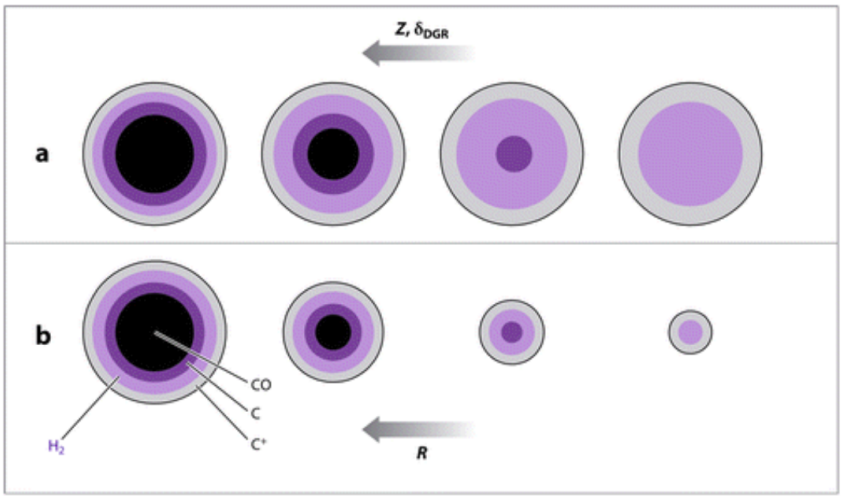

FIGURE 1.2. Interaction of H_2 in light purple, CO in black, C^+ and C in a clump in a uniform radiation field. Panel a: Decreasing metallicity with a cloud of constant size. Panel b: Change in cloud size or density while metallicity remains constant. Image: Bolatto et al. (2013)

In contrast to what is expected of the classical onion-shaped structure of PDRs (e.g., Hollenbach and Tielens, 1999),more recent simulations suggest that neutral carbon emission appears to be widespread in H_2 clouds (e.g., Offner et al., 2014; Glover and Clark, 2016; Bisbas et al., 2017). Observations that support this scenario include large-scale maps of CO isotopologues and [CI] lines of star-forming regions in the Small and Large Magellanic Clouds (Requena-Torres et al., 2016; Okada et al., 2019) , and ρ Ophiuchi (Kulesa et al., 2005) and Orion giant molecular clouds. For the latter, the emission of [CI](1-0) is measured to be optically thin ($\tau_{[CI]} \sim 0.1 - 0.3$) and coincide with the emission of the 12CO line and the lines of ^{13}CO(1-0) (Ikeda et al., 2002; Shimajiri et al., 2013). On the other hand, in nearby star-forming galaxies and starbursts, observations at the kiloparsec scale suggest that [CI] may be a good tracer for cold H2 gas like CO, but not superior (e.g., Israel et al., 2015; Crocker et al., 2019).

In combination with multiple CO transitions, the pair of [CI] lines can be used to constrain the physical properties of the molecular gas. Valentino et al. (2020a), based on Large Velocity Gradient (LVG) modeling of the CO+[CI] spectral line energy distributions (SLEDs), find that to reproduce the observed SLEDs of $z \sim 1$ main-sequence galaxies at least two molecular gas components are necessary: one that is relatively diffuse ($n_{H_2} \approx 10^2$ cm^{-3}, $T_{kin} \approx 45$ K) and one that is dense ($n_{H_2} \approx 10^4$ cm^{-3}, $T_{kin} \approx 45$ K). In a similar analysis of BX610, a massive, main-sequence galaxy at $z \approx 2$, Brisbin et al. (2019) also find that two molecular gas components are an option, with the high density one heated either by intense star formation or low-velocity C-shocks. There is certainly much more work to be done to constrain the molecular gas properties of galaxies across cosmic time, and the combination of CO+[CI] SLEDs is one promising tool to achieve this goal. Harrington (2020), according to their non-LTE radiative transfer model of the [CI] lines for starburst galaxies at peak star formation, suggests that these lines are optically thin, which is important for reliable calibrations for the column density. of carbon gas and the total molecular gas mass.

The subject of study is Q1700-MD94 (hereafter MD94), a massive ($M_\star = 1.5 \times 10^{11}\ M_\odot$), star-forming (SFR $= 271\ M_\odot$ yr^{-1}) system at $z = 2.333$ (Tacconi et al., 2013) located at the

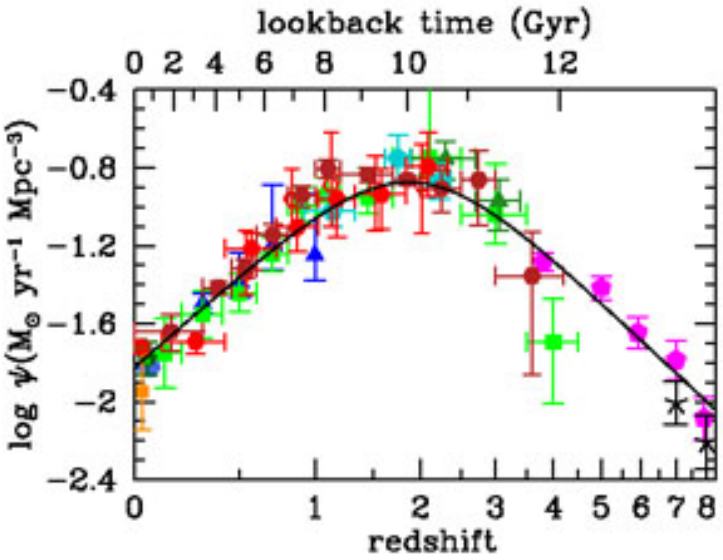

FIGURE 1.3. Star formation rate density versus redshift. The top axis shows the lookback time in Gyr. The points are different observations made in the infrared and ultraviolet range. The peak of star formation is observed at $z \sim 2$ approximately. Image: Madau and Dickinson (2014)

massive end of the main-sequence of galaxies at $z \sim 2$ (e.g., Whitaker et al., 2012)

To give some context about MD94, we can revisit the history of cosmic star formation activity (see Fig. 1.3). Three important periods stand out: From approximately $z > 5$ on wards we find an epoch in which galaxies had a large deposit of molecular gas to form stars so they grow and evolve. At approximately $z \sim 2$, galaxies reach a star formation peak, an epoch known as "galaxy assembly", where they manage to form more than 50% of the stars we see today. Then, from $z < 2$ to $z = 0$, galaxies experience a decline in their star formation activity (Madau and Dickinson, 2014). We delve into the molecular gas that helps to elucidate an important clue of what is happening with this problem.

Depending on the cosmic epoch, galaxies can be classified according to their mass and star formation rate (see Fig. 1.4). Three areas stand out: The first is the sector of the "starburst" galaxies characterized by galaxies that have a high star formation rate per unit stellar mass. Then, the "main sequence", where the production of stars is "normal or typical" as observed for their respective redshift. Finally, there are the "quiescent galaxies" that almost do not form stars because they have used up all their fuel (the molecular gas).

Due to ALMA and the improved capabilities of IRAM/NOEMA the number of high redshift galaxies observed with the [CI] emission lines has been increasing (e.g., Bothwell et al., 2017; Lee et al., 2021). Observations are no longer restricted to bright quasars or submillimeter galaxies (e.g., Weiß et al., 2003, 2005; Walter et al., 2011). The goal of our work is to determine the molecular gas properties of MD94 based on the emission of the pair of

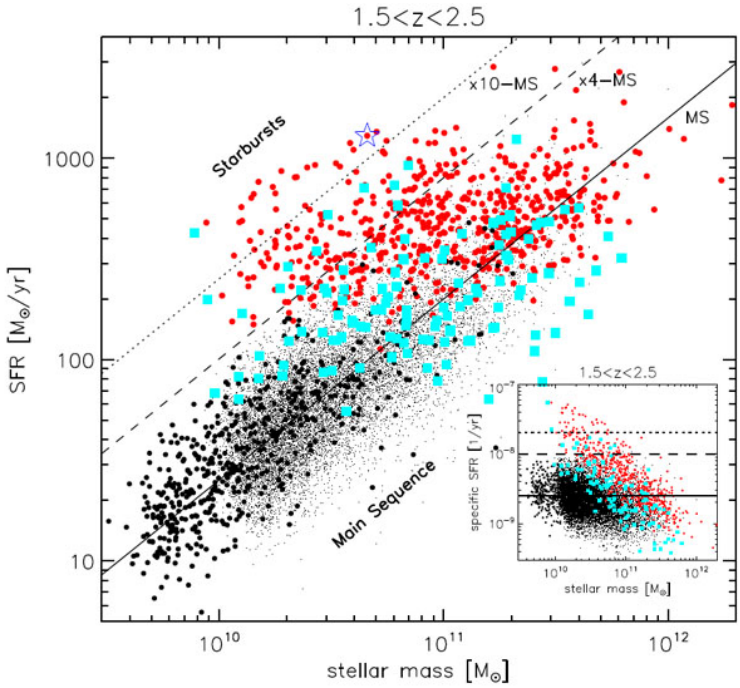

FIGURE 1.4. Solar masses versus star formation rate (SFR) at $1.5 < z < 2.5$. Data are different galaxy samples. The solid black line shows the area of the main sequence, galaxies that have a normal or typical star formation rate.We can distinguish two other regions: a region of dormant galaxies (below the main sequence) where star formation stopped and the stellar explosion zone, where galaxies that have a lot of dust and gas are located to form a large number of new stars. Small box: the same relationship but based on specific SFR. Image: Rodighiero et al. (2011)

[CI] lines, plus three lines of CO(1-0,3-2,7-6) (Bolatto et al., 2015; Tacconi et al., 2013). Having all these transitions represents an advantage to be able to characterize more precisely the molecular gas of a massive, main-sequence galaxy at the peak of cosmic star formation activity.

Chapter 2

Observations

We observed MD94 with NOEMA located in the French Alps. On August 31, 2017, we used the 2 mm band for a total of 7.5 hours to target the [CI](1-0) line located at an observed frequency of $\nu_{\rm obs} = 147.8$ GHz. Then, starting on September 1, 2017, we used the 1 mm band for a total of 14.3 hours to observe the [CI](2-1) and CO(7-6) lines centered at an observed frequency of $\nu_{\rm obs} = 243.0$ GHz. All observations were carried out in NOEMA D array configuration, which is the most compact one.

The data were calibrated in CLIC with help from the staff in Grenoble. After calibration, we used the software MAPPING2[1] to clean and image the data using natural weighting. For the [CI](1-0) cube the resulting synthesized beam was $3.0'' \times 2.2''$ ($\sim 24.9 \times 18.2$ kpc) and the noise level was 0.25 mJy beam^{-1} in 100 km s^{-1}. For the [CI](2-1) and CO(7-6) cube the resulting beam was $1.7'' \times 1.3''$ ($\sim 14.1 \times 10.7$ kpc) and the noise level was 0.31 mJy beam^{-1} in 75 km s^{-1}. In the latter cube we detected continuum emission, which was subtracted from the spectra before any line analysis was done.

[1] CLIC and MAPPING2 are part of the GILDAS package (Guilloteau and Lucas, 2000). http://www.iram.fr/IRAMFR/GILDAS

Chapter 3

Results

3.1 Detection of the [CI](1-0), [CI](2-1) and CO(7-6) transitions and the dust continuum

The spectra of the [CI](1-0), [CI](2-1) and CO(7-6) lines observed in MD94 are shown in the top panel of Fig. 3.1. The continuum emission detected under the [CI](2-1) and CO(7-6) lines was determined and subtracted based on the emission from the frequency channels below and above the CO(7-6) and [CI](2-1) lines, respectively. The continuum flux measured at (rest-frame) 240 GHz is 2.5 ± 0.8 mJy. The [CI](1-0), [CI](2-1) and CO(7-6) lines are detected with signal-to-noise ratios of $S/N \approx 4$, 6 and 10, respectively. We fit a single Gaussian profile to each line. The measured linewidths (FWHM) and integrated fluxes are listed in Table 1. The redshift of the source derived from the central frequency of the Gaussian fit is similar to the value of $z = 2.33$ measured from observations of the Hα and CO(3-2) lines by Tacconi et al. (2013).

The bottom panels of Fig. 3.1 show the integrated intensity maps. We (barely) spatially resolve MD94 in the [CI](2-1) and CO(7-6) line emission. Similar to the spatial distribution observed in the CO(1-0) line emission by Bolatto et al. (2015), the source is elongated in the N-S direction. The deconvolved sizes are $1.4'' \times 0.7''$ and $1.2'' \times 0.61''$ for the [CI](2-1) and CO(7-6) lines, respectively. These sizes are comparable to the deconvolved source size of $1.3'' \times 1.0''$ measured from the CO(1-0) line emission (Bolatto et al., 2015).

We calculated the luminosities of the [CI] and CO lines following Solomon and Vanden Bout (2005). For the luminosity distance and other physical parameters we use a standard cosmology ($H_0 = 67.4$ km s^{-1} Mpc^{-1}, $\Omega_M = 0.315$, $\Omega_\Lambda = 0.685$ Planck Collaboration et al., 2020).

TABLE 3.1. Q1700-MD94 derived values

Line	FWHM [km s^{-1}]	$S\Delta v$ [Jy km s^{-1}]	Reference
[CI](1-0)	482 ± 124	0.49 ± 0.13	This work
[CI](2-1)	383 ± 75	0.92 ± 0.15	This work
CO(1-0)	296 ± 66	0.14 ± 0.01	Bolatto et al. (2015)
CO(3-2)	294 ± 49	1.52 ± 0.17	Bolatto et al. (2015)
CO(7-6)	518 ± 61	1.67 ± 0.17	This work
Continuum		Flux density [mJy]	
$S_{240\ \mathrm{GHz}}$		2.5 ± 0.8	This work

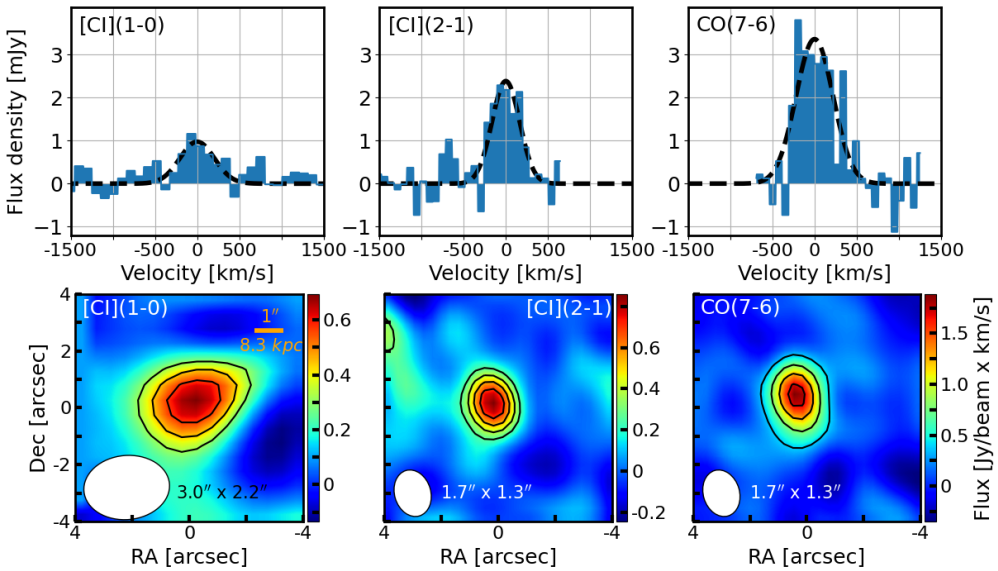

FIGURE 3.1. *(Top)* From left to right, [CI](1-0), [CI](2-1), and CO(7-6) spectra of MD94. The black-dashed lines show the single Gaussian fit to the spectra. The FWHM and integrated fluxes are listed in Table 1. *(Bottom)* From left to right, integrated intensity maps of the [CI](1-0), [CI](2-1), and CO(7-6) emission of MD94. Contours start at 2σ and increase in steps of 1σ. The NOEMA synthesized beam is shown in the lower left corner.

3.2 The molecular gas mass of MD94

The molecular gas mass of MD94 can be measured from available observations of the CO(1-0) line (Bolatto et al., 2015), the dust continuum, and the pair of [CI] lines (this work). In all cases it is necessary to make assumptions about the abundance of the tracer to convert the luminosity into a molecular gas mass.

According to the mass-metallicity relation and parameterization in Genzel et al. (2015), MD94 has a metallicity of $12 + \log(\mathrm{O/H}) = 8.64$, which is roughly the solar value (Asplund et al., 2004). Following Tacconi et al. (2018), for the metallicity of MD94 the CO(1-0) metallicity dependent conversion factor is $\alpha_{\mathrm{CO}} = 4.5\ M_\odot\ (\mathrm{K\ km\ s^{-1} pc^2})^{-1}$ (this includes the 1.36 helium correction factor). Based on this, and the CO(1-0) luminosity in Bolatto et al. (2015), the molecular gas mass in MD94 is $M_{\mathrm{mol}} = 1.7 \times 10^{11}\ M_\odot$.

Alternatively, the interstellar medium (ISM) gas mass can be estimated from the single dust continuum measurement at (rest-frame) 240 GHz (see Table 3.1). Following Eq. (15) in Scoville et al. (2016), we measure a gas mass in MD94 of $M_{\mathrm{ISM}} \approx 7 \times 10^{10}\ M_\odot$ [1]. This total gas mass is a factor of ~ 2 lower than the CO-based molecular gas mass, which is expected given the multiple assumptions both methods require.

Finally, the atomic carbon mass based on the [CI](1-0) line can be calculated following, e.g., Weiß et al. (2005):

$$M_{[\mathrm{CI}]} = 5.706 \times 10^{-4} Q(T_{\mathrm{ex}}) \frac{1}{3} \mathrm{e}^{\frac{23.6}{T_{\mathrm{ex}}}} L'_{[\mathrm{CI}](1-0)}\ M_\odot, \tag{3.1}$$

where T_{ex} is the excitation temperature and $Q(T_{\mathrm{ex}}) = 1 + 3\mathrm{e}^{-T_1/T_{\mathrm{ex}}} + 5\mathrm{e}^{-T_2/T_{\mathrm{ex}}}$ is the partition function. Here $T_1 = 23.6$ K and $T_2 = 62.5$ K are the energies above ground state.

[1] This calculation assumes a dust-to-gas ratio appropriate for massive, star-forming galaxies, and includes a Rayleigh–Jeans correction calculated for a dust temperature of $T = 35$ K. This temperature is consistent with the gas temperature derived from the ratio of the [CI] lines in MD94, and also the typical dust temperature measured in massive, main-sequence galaxies at $z \approx 2$ (e.g., ?Genzel et al., 2015; Schreiber et al., 2018)

The advantage of having detected the pair of [CI] lines in MD94, is that we can use their brightness ratio to directly measure the excitation temperature $T_{\rm ex}$ in the optically thin limit. In MD94 we measure a [CI] line ratio of $R = L'_{[\rm CI](2-1)}/L'_{[\rm CI](1-0)} = 0.7$. Following Stutzki et al. (1997), the excitation temperature in MD94 is

$$T_{\rm ex} = 38.8 \times \ln\left(\frac{2.11}{\rm R}\right)^{-1} \approx 35 \text{ K}. \quad (3.2)$$

This value is close to the average [CI] excitation temperature of $T_{\rm ex} \approx 30$ K measured in the sample of dusty starbursts and QSOs in Walter et al. (2011), and about ∼10 K warmer than the average excitation temperature measured in main-sequence galaxies at $z \sim 1$ (Valentino et al., 2020b). In the absence of one of the two [CI] lines, it is a common approach to assume the dust temperature as a proxy for the excitation temperature. In the case of MD94, the [CI]-based $T_{\rm ex}$ is comparable to the typical dust temperature of $T_{\rm dust} \approx 32$ K measured in massive ($M_\star \approx 10^{11} - 10^{11.5}\ M_\odot$), main-sequence star-forming galaxies at $z \approx 2$ (**?**Genzel et al., 2015; Schreiber et al., 2018).

From Eq. (1), and the excitation temperature in Eq. (2), the resulting atomic carbon mass in MD94 is $M_{\rm [CI]} = 9.2 \times 10^6\ M_\odot$. To convert this quantity into a molecular gas mass we need to assume an atomic carbon abundance relative to H_2, i.e., $X_{\rm CI} = M_{\rm CI}/6M_{\rm H_2}$. There is a wide range of $X_{\rm CI}$ values indirectly measured or assumed for different galaxy types and cosmic epochs. Valentino et al. (2018), using a homogenized method to compare the molecular gas masses derived from archival dust, low-J CO, and [CI](1-0) line observations, find that $X_{\rm CI}$ varies from $\sim 1 - 3 \times 10^{-5}$ in $z \sim 1$ main-sequence galaxies, $\sim 3 - 8 \times 10^{-5}$ in SMGs at $z \sim 2$, and $\sim 3 - 10 \times 10^{-5}$ in nearby galaxies (note that $M_{\rm H_2}$ values in Valentino et al. (2018) do not include the helium contribution). For MD94, if we compare the atomic carbon mass to the average molecular gas mass from the CO(1-0) line and dust continuum estimates, we find $X_{\rm CI,MD94} \approx 1.3 \times 10^{-5}$. This value is within the range of abundances derived by Valentino et al. (2018), and comparable to the typically assumed abundance for massive, high redshift systems of $X_{\rm CI} \approx 3 \times 10^{-5}$ (e.g., Weiß et al., 2005; Alaghband-Zadeh et al., 2013; Popping et al., 2017). In summary, for reasonable assumptions on $\alpha_{\rm CO}$, dust-to-gas ratio, and $X_{\rm CI}$ for a massive, near solar metallicity galaxy like MD94, we find that the molecular gas mass measurements based on the CO(1-0), dust continuum, and [CI](1-0) transitions are comparable (e.g., within a factor of ∼ 2).

Finally, the molecular gas mass in MD94 implies this galaxy has a molecular gas fraction of $\mu = M_{\rm mol}/M_\star \approx 1$ and a molecular gas depletion timescale of $t_{\rm dep} = M_{\rm mol}/{\rm SFR} \approx 0.5$ Gyr. Both quantities are characteristic of massive, main-sequence galaxies at $z \sim 2$ (Tacconi et al., 2018).

3.3 [CI] and CO Spectral Line Energy Distributions

The analysis of the SLED of the pair of [CI] and CO lines can provide valuable insights into the physical conditions of the molecular gas. Fig. 3.2 shows the CO and [CI] SLEDs of MD94 compared to other nearby and high-redshift galaxies. Given the strong link observed between the shape of the SLED and the SFR surface density $\Sigma_{\rm SFR}$ (e.g., Narayanan and Krumholz, 2014), we include galaxies that have $\Sigma_{\rm SFR}$ values that range from $\sim 1\times$ (e.g., BX610, mean BzK $z \sim 1.5$ galaxies) to $\sim 150\times$ (e.g., Cloverleaf quasar) that of MD94 ($\Sigma_{\rm SFR} \approx 2\ M_\odot\ {\rm yr}^{-1}\ {\rm kpc}^{-2}$; Tacconi et al., 2013).

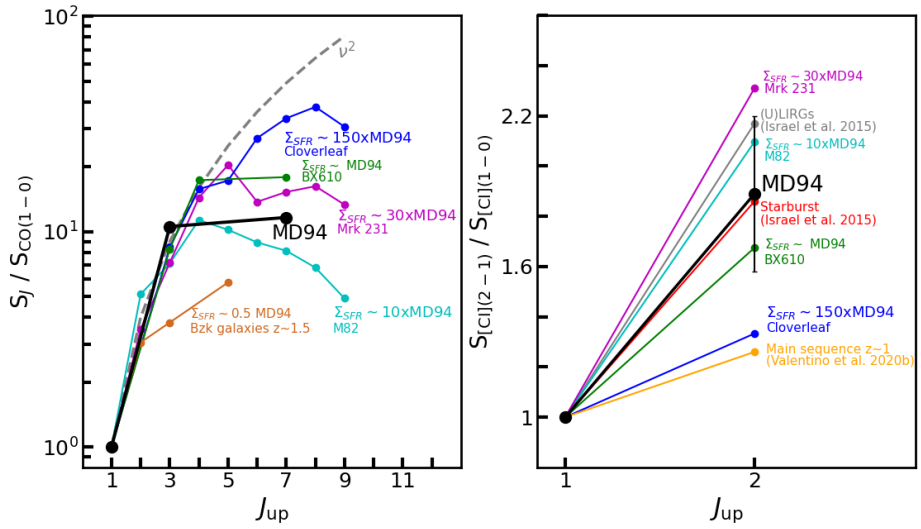

FIGURE 3.2. CO (*left*) and [CI] (*right*) SLEDs of MD94 (black), and other nearby and high-redshift systems. We indicate (when available) the SFR surface density in terms of the value measured in MD94 ($\Sigma_{SFR} \approx 2\ M_\odot\ yr^{-1}\ kpc^{-2}$). The references for the ancillary data shown are the following: Mrk 231 (van der Werf et al., 2010), M82 (Kamenetzky et al., 2012), and Cloverleaf (Barvainis et al., 1997). In addition to these, we added BX610 (Brisbin et al., 2019), average values for (U)LIRGs and starbursts (Israel et al., 2015), and the mean value for main-sequence galaxies at $z \sim 1$ (Valentino et al., 2020b), and BzK main-sequence galaxies at $z \sim 1.5$ (Daddi et al., 2015). The dashed dark grey line shows constant brightness temperature on the Rayleigh–Jeans scale ($S \propto \nu^2$).

The integrated flux ($S_{CO}\Delta v$) ratio between the $J = 3-2$ and $J = 1-0$ in MD94 is ~ 10 (Bolatto et al., 2015), which is consistent with its high levels of star formation activity, similar to the examples of M82 (in the figure) and NGC253 (Bradford et al., 2003). It is also consistent with the high integrated line ratios observed in AGN galaxies, such as Mrk 231 and the Cloverleaf quasar (in the figure). It is important to note that, from the observed broad Hα line profile (Erb et al., 2006), MD94 could host an AGN possibly accompanied by an outflow.

The inclusion of the CO(7-6) line is key to further differentiate the gas excitation conditions in MD94 from other systems, and also to search for an additional denser and/or warmer component of molecular gas present. In that sense, the (partially complete) SLED of MD94 from $J = 1$ to $J = 7$ better resembles the shape of the SLED of nearby AGN galaxy Mrk 231 ($\Sigma_{SFR} \sim 30 \times \Sigma_{SFR,MD94}$), than the nearby starburst M82 ($\Sigma_{SFR} \sim 10 \times \Sigma_{SFR,MD94}$) that peaks at $J = 4$ and then declines. It is also similar to the SLED of BX610, another massive, main-sequence galaxy at $z \approx 2$ with a comparable value of Σ_{SFR} and showing no or weak signs of AGN activity (Bolatto et al., 2015; Brisbin et al., 2019). For the latter, LVG models suggest that at least a second, higher-density PDR component or a low-velocity C shock heated component is needed to better reproduce the CO+[CI] SLED (Brisbin et al., 2019).

The right panel of Fig. 3.2 shows the [CI] SLED of MD94. We also include most of the systems in the left panel plus the average [CI] SLED observed in main-sequence galaxies at $z \sim 1$ (Valentino et al., 2018) and nearby starbursts and (U)LIRGs (Israel et al., 2015). MD94 has a [CI](2-1)/[CI](1-0) integrated flux ratio of ≈ 1.9, similar to the typical value found in nearby starbursts (Israel et al., 2015), and slightly higher than BX610 (Brisbin et al., 2019).

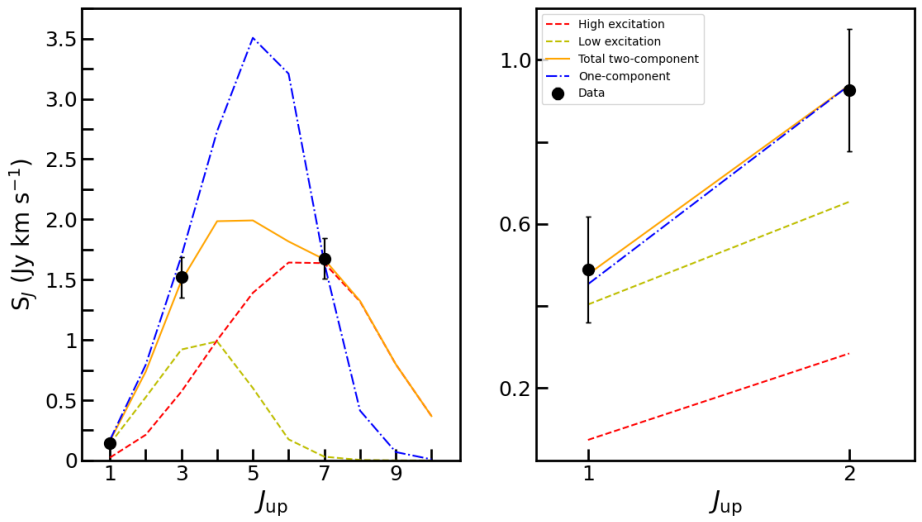

FIGURE 3.3. LVG RADEX modeling of the CO (left) and [CI] (right) SLEDs. The blue line shows the best RADEX single-component model ($T = 41$ K, $n_{H_2} = 8.5 \times 10^3$ cm^{-3}). The orange line shows the best two-component model, which is the combination of a low- ($T = 34$ K, $n_{H_2} = 3.1 \times 10^3$ cm^{-3}; green) and a high-excitation ($T = 137$ K, $n_{H_2} = 1.6 \times 10^4$ cm^{-3}; red) components.

The fact that MD94 shows a [CI] SLED that is more excited than, for instance, the Cloverleaf QSO ($\Sigma_{SFR} \sim 150 \times \Sigma_{SFR,MD94}$), reveals the complexity of the molecular gas in these systems in terms of excitation properties and structure. It also suggests that the molecular gas component dominating the mid- and high-J CO emission is different from that powering the [CI] line emission. We further investigate the shape of the CO+[CI] SLEDs in the next section.

3.4 Large Velocity Gradient modeling

To look deeper into the physical conditions of the gas that produce the CO and [CI] line emission in MD94, we use a set of LVG models generated by the one-dimensional, non-LTE radiative transfer code RADEX (van der Tak et al., 2007). RADEX models mainly depend on three input parameters: gas kinetic temperature (T_K), molecular hydrogen density (n_{H2}), and the CO (or C) column density per unit velocity gradient ($N(CO)/dV$ or $N(C)/dV$). To model the CO+[CI] SLED of MD94 we generated a grid of models varying the H_2 density from $n_{H_2} = 10^2$ to 10^5 cm^{-3}, and the kinetic temperature from $T_{kin} = 10$ to 200 K. Following the LVG modeling of Israel et al. (2015), and to avoid overfitting the limited CO SLED of MD94, we fixed the CO gradient to $N(CO)/dV = 10^{17}$ cm^{-2} (km s^{-1})$^{-1}$, but note that varying $N(CO)/dV$ in the range $10^{17} - 10^{18}$ (km s^{-1})$^{-1}$ only changes the results by less than 20%. We also assumed an abundance ratio of C:CO of 1:4, consistent with abundance ratios found in nearby star-forming galaxies (Crocker et al., 2019) and the $z \sim 2$ main-sequence galaxy BX610 (Brisbin et al., 2019). The background temperature was set to $2.73 \times (1 + 2.33) = 9$ K.

We simultaneously compare the CO and [CI] SLEDs of MD94 with the set of RADEX models, calculating the goodness of the fit based on the reduced-χ^2 value. We started with models based on a single molecular gas component. Of these, the one that best reproduce the data (reduced-$\chi^2 \approx 3$) has a gas density of $n_{H_2} = 8.5 \times 10^3$ cm^{-3} and a temperature of $T_{kin} = 41$ K. Next, we fitted the CO+[CI] SLEDs of MD94 using a two-component model. This is not

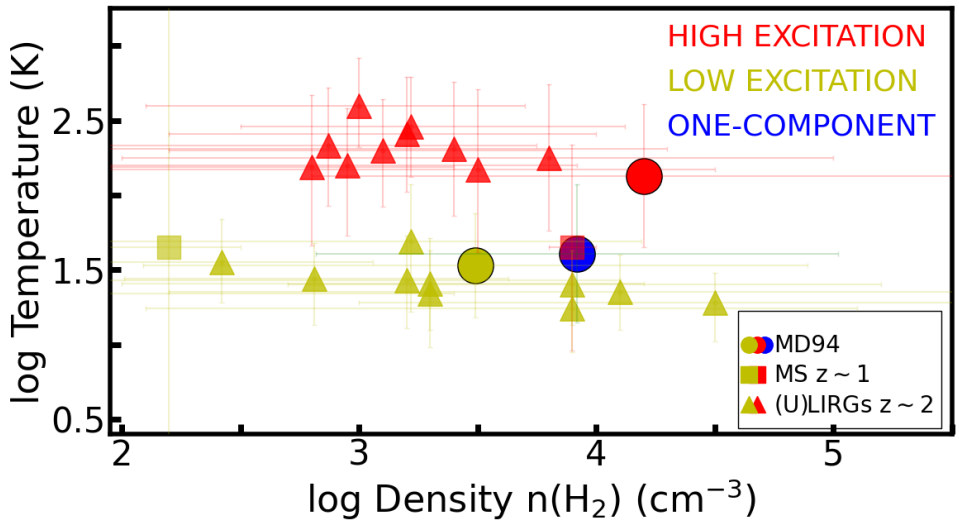

FIGURE 3.4. Kinetic temperature and molecular gas density from the best RADEX LVG one-component (blue circle) and two-component model (red and green circles) fitted to the CO and [CI] SLEDs of MD94. We also show the derived values for lensed ULIRGs at $z \sim 2-3$ (Yang et al., 2017; Cañameras et al., 2018) (triangles), and the average value for main-sequence galaxies at $z \sim 1$ (Valentino et al., 2020a) (squares).

uncommon for nearby galaxies and high redshift systems (e.g., Mashian et al., 2015; Daddi et al., 2015; Cañameras et al., 2018; Valentino et al., 2020a), where a combination of a low-excitation (or cold) and a high-excitation (or warm) component are needed to reproduce the observed SLEDs. We find that MD94 is not the exception, and that a two component model with a low ($T_{\rm kin} = 34$ K, $n_{\rm H_2} = 3.1 \times 10^3$ cm^{-3}) and a high ($T_{\rm kin} = 137$ K, $n_{\rm H_2} = 1.6 \times 10^4$ cm^{-3}) excitation component produces the best overall fit, with a reduced-$\chi^2 \approx 2$.

Fig. 3.3 shows the best one- and two-component RADEX LVG models overplotted on the CO+[CI] SLED of MD94. The best single-component model is shown as a blue dotted-dashed line and peaks at $J = 5$. Unfortunately, we do not have observational constraints around this peak. The best two-component model is shown as a green and red dashed curves, for the low and high excitation component, respectively. In this case, the fraction of the [CI] emission contributed by the low-excitation component is dominant ($\sim 80\%$), similar to what is found in nearby star-forming galaxies (Crocker et al., 2019). For CO, there is a steady increase in the contribution from the high-excitation component, becoming dominant at $J \geq 4$. As expected, the contribution from the low-excitation component to the $J = 7$ line is minimal ($\lesssim 5\%$).

3.4.1 How does the physical properties of the molecular gas of MD94 compare to other galaxies at $z \sim 1-2$

There are two other main-sequence galaxies at $z \approx 2$ with similar stellar mass as MD94 ($\sim 10^{11}\ M_\odot$) that have been studied based on the combination of the [CI] and CO lines and the dust continuum. These galaxies are BX610 (Tacconi et al., 2013; Bolatto et al., 2015; Brisbin et al., 2019) and GS30274 (Popping et al., 2017; Talia et al., 2018). While the former share the average molecular gas properties of main-sequence galaxies at $z \sim 2$ (Tacconi et al., 2018), the latter shows a very short depletion time ($t_{\rm dep} \approx 100$ Myr), compact structure ($r_{\rm e} \approx 2$ kpc), a

powerful AGN-driven outflow (e.g., Förster Schreiber et al., 2014; Genzel et al., 2014; Davies et al., 2020), and it is considered to be in the process of quenching (Popping et al., 2017).

Massive, main-sequence galaxies at $z \sim 2$ are expected to experience star formation quenching as the fraction of quiescent galaxies with stellar masses similar to MD94 increases from $\sim 20\%$ at $z \sim 2-3$ to $\sim 70\%$ at $z \sim 1$ (e.g. Muzzin et al., 2013). From the standpoint of the global molecular gas fraction and depletion timescale, MD94 is closer to BX610 than GS30274, and does not show evident signatures for quenching of its star formation activity. This could be, of course, a result of the poor spatial resolution of our observations that washes out any evidence of quenching mechanisms operating in the central region around the AGN. The only similarity we find between MD94 and the quenching galaxy GS30274 is that the LVG modeling of MD94 suggests the presence of warm ($\sim$ 130 K) and dense ($\sim 10^4$ cm^{-3}) gas similar to that observed in GS30274. As Fig. 3.4 shows, the high-excitation gas component in MD94 is comparable in density, but warmer, to the main high-excitation component in main-sequence galaxies at $z \sim 1$ (Valentino et al., 2020a). It is also similar in temperature, but denser, than the high-excitation component detected in highly-lensed starbursts at $z \sim 2$ (Yang et al., 2017; Cañameras et al., 2018). For MD94, this could be the result of highly-excited gas in the central region as a result, for example, of a compaction event. However, the fact that the deconvolved sizes of MD94 in the CO(1-0) and CO(7-6) line emission are comparable, suggests that the dense gas excited by intense star formation activity is well mixed with cold and diffuse molecular gas throughout the disk. Only high-spatial resolution observations of the molecular gas in multiple transitions, which can be achieved for example by NOEMA upgraded capabilities (e.g., baseline extension), could provide an answer in the near future.

Chapter 4

Conclusions

We present new NOEMA observations of the [CI](1-0), [CI](2-1) and CO(7-6) transitions of the massive, main-sequence galaxy Q1700-MD94 at $z \approx 2.3$. Combined with ancillary observations of the CO(1-0) (Bolatto et al., 2015) and the CO(3-2) (Tacconi et al., 2013) lines, we have characterized the molecular gas properties of MD94. We highlight the following points:

- We find that for a reasonable set of assumptions for a massive galaxy such as MD94, the molecular gas mass estimates from the dust continuum, the CO(1-0), and the [CI](1-0) line are consistent within a factor of ~ 2. At least for this system, our analysis shows that the [CI](1-0) transition is a reliable alternative to the CO(1-0) line to study the molecular gas properties of the low-excitation gas.

- The CO SLED of MD94 shows excitation properties similar to BX610, another massive galaxy at $z \approx 2$ with a comparable SFR surface density ($\Sigma_{\rm SFR} \approx 2\ M_\odot\ {\rm yr}^{-1}\ {\rm kpc}^{-2}$). Compared to nearby systems, the CO SLED shape is closer to that of Mrk231 ($\Sigma_{\rm SFR} \approx 30 \times \Sigma_{\rm SFR,MD94}$) than M82 ($\Sigma_{\rm SFR} \approx 10 \times \Sigma_{\rm SFR,MD94}$), perhaps because MD94 also hosts an AGN. The [CI] SLED of MD94 is also comparable to that of BX610 and the mean [CI] SLED of nearby starburst galaxies (Israel et al., 2015).

- Based on LVG models from RADEX, we simultaneously fit the CO and [CI] SLEDs of MD94. The best model involves a low-excitation ($T_{\rm kin} = 34$ K, $n_{\rm H_2} = 3.1 \times 10^3$ cm^{-3}) and a high-excitation ($T_{\rm kin} = 137$ K, $n_{\rm H_2} = 1.6 \times 10^4$ cm^{-3}) component. We observed that the [CI] SLED of MD94 is dominated by the low-excitation component, while in the CO SLED the contribution from the high-excitation component steadily increases and dominates the CO(7-6) line emission.

- MD94 exhibits molecular gas properties (e.g., $f_{\rm gas} \approx 1$, $t_{\rm dep} \approx 0.5$ Gyr) similar to those observed in main-sequence star-forming galaxies at $z \sim 2$ (e.g. Tacconi et al., 2018). The fact that the deconvolved sizes of the disk in the CO(7-6) and CO(1-0) line emission are comparable, suggests that the star formation activity that heat the gas is widely distributed, and not concentrated in a compact central region. Future observations that can spatially resolve the molecular gas properties of MD94 are needed to further confirm this scenario.

Bibliography

Alaghband-Zadeh, S., Chapman, S. C., Swinbank, A. M., Smail, I., Danielson, A. L. R., Decarli, R., Ivison, R. J., Meijerink, R., Weiss, A., and van der Werf, P. P. (2013). "Using [C I] to probe the interstellar medium in z $\sim$ 2.5 sub-millimeter galaxies." , *435*(2), 1493–1510.

Asplund, M., Grevesse, N., Sauval, A. J., Allende Prieto, C., and Kiselman, D. (2004). "Line formation in solar granulation. IV. [O I], O I and OH lines and the photospheric O abundance." , *417*, 751–768.

Barvainis, R., Maloney, P., Antonucci, R., and Alloin, D. (1997). "Multiple CO Transitions, C I, and HCN from the Cloverleaf Quasar." , *484*(2), 695–701.

Bisbas, T. G., van Dishoeck, E. F., Papadopoulos, P. P., Szűcs, L., Bialy, S., and Zhang, Z.-Y. (2017). "Cosmic-ray Induced Destruction of CO in Star-forming Galaxies." , *839*(2), 90.

Bolatto, A. D., Warren, S. R., Leroy, A. K., Tacconi, L. J., Bouché, N., Förster Schreiber, N. M., Genzel, R., Cooper, M. C., Fisher, D. B., Combes, F., García-Burillo, S., Burkert, A., Bournaud, F., Weiss, A., Saintonge, A., Wuyts, S., and Sternberg, A. (2015). "High-resolution Imaging of PHIBSS z $\sim$ 2 Main-sequence Galaxies in CO J = 1 $\rightarrow$ 0." , *809*(2), 175.

Bolatto, A. D., Wolfire, M., and Leroy, A. K. (2013). "The CO-to-H_2 Conversion Factor." , *51*(1), 207–268.

Bothwell, M. S., Aguirre, J. E., Aravena, M., Bethermin, M., Bisbas, T. G., Chapman, S. C., De Breuck, C., Gonzalez, A. H., Greve, T. R., Hezaveh, Y., Ma, J., Malkan, M., Marrone, D. P., Murphy, E. J., Spilker, J. S., Strandet, M., Vieira, J. D., and Weiß, A. (2017). "ALMA observations of atomic carbon in z $\sim$ 4 dusty star-forming galaxies." , *466*(3), 2825–2841.

Bradford, C. M., Nikola, T., Stacey, G. J., Bolatto, A. D., Jackson, J. M., Savage, M. L., Davidson, J. A., and Higdon, S. J. (2003). "CO (J=7–¿6) Observations of NGC 253: Cosmic-Ray-heated Warm Molecular Gas." , *586*(2), 891–901.

Brisbin, D., Aravena, M., Daddi, E., Dannerbauer, H., Decarli, R., González-López, J., Riechers, D., and Wagg, J. (2019). "Neutral carbon and highly excited CO in a massive star-forming main sequence galaxy at z = 2.2." , *628*, A104.

Cañameras, R., Yang, C., Nesvadba, N. P. H., Beelen, A., Kneissl, R., Koenig, S., Le Floc'h, E., Limousin, M., Malhotra, S., Omont, A., and Scott, D. (2018). "Planck's dusty GEMS. VI. Multi-J CO excitation and interstellar medium conditions in dusty starburst galaxies at z = 2-4." , *620*, A61.

Carilli, C. L., and Walter, F. (2013). "Cool Gas in High-Redshift Galaxies." , *51*(1), 105–161.

Crocker, A. F., Pellegrini, E., Smith, J. D. T., Draine, B. T., Wilson, C. D., Wolfire, M., Armus, L., Brinks, E., Dale, D. A., Groves, B., Herrera-Camus, R., Hunt, L. K., Kennicutt, R. C.,

Murphy, E. J., Sandstrom, K., Schinnerer, E., Rigopoulou, D., Rosolowsky, E., and van der Werf, P. (2019). "[C I](1-0) and [C I](2-1) in Resolved Local Galaxies." , *887*(1), 105.

Daddi, E., Dannerbauer, H., Liu, D., Aravena, M., Bournaud, F., Walter, F., Riechers, D., Magdis, G., Sargent, M., Béthermin, M., Carilli, C., Cibinel, A., Dickinson, M., Elbaz, D., Gao, Y., Gobat, R., Hodge, J., and Krips, M. (2015). "CO excitation of normal star-forming galaxies out to z = 1.5 as regulated by the properties of their interstellar medium." , *577*, A46.

Davies, R. L., Förster Schreiber, N. M., Lutz, D., Genzel, R., Belli, S., Shimizu, T. T., Contursi, A., Davies, R. I., Herrera-Camus, R., Lee, M. M., Naab, T., Price, S. H., Renzini, A., Schruba, A., Sternberg, A., Tacconi, L. J., Übler, H., Wisnioski, E., and Wuyts, S. (2020). "From Nuclear to Circumgalactic: Zooming in on AGN-driven Outflows at z $\sim$ 2.2 with SINFONI." , *894*(1), 28.

Draine, B. T. (2011). *Physics of the Interstellar and Intergalactic Medium*.

Dyson, J. E., and Williams, D. A. (1997). *The physics of the interstellar medium*.

Erb, D. K., Steidel, C. C., Shapley, A. E., Pettini, M., Reddy, N. A., and Adelberger, K. L. (2006). "Hα Observations of a Large Sample of Galaxies at z ~2: Implications for Star Formation in High-Redshift Galaxies." , *647*(1), 128–139.

Ferrière, K. M. (2001). "The interstellar environment of our galaxy." *Reviews of Modern Physics*, *73*(4), 1031–1066.

Förster Schreiber, N. M., Genzel, R., Newman, S. F., Kurk, J. D., Lutz, D., Tacconi, L. J., Wuyts, S., Bandara, K., Burkert, A., Buschkamp, P., Carollo, C. M., Cresci, G., Daddi, E., Davies, R., Eisenhauer, F., Hicks, E. K. S., Lang, P., Lilly, S. J., Mainieri, V., Mancini, C., Naab, T., Peng, Y., Renzini, A., Rosario, D., Shapiro Griffin, K., Shapley, A. E., Sternberg, A., Tacchella, S., Vergani, D., Wisnioski, E., Wuyts, E., and Zamorani, G. (2014). "The Sins/zC-Sinf Survey of z ~2 Galaxy Kinematics: Evidence for Powerful Active Galactic Nucleus-Driven Nuclear Outflows in Massive Star-Forming Galaxies." , *787*(1), 38.

Genzel, R., Förster Schreiber, N. M., Lang, P., Tacchella, S., Tacconi, L. J., Wuyts, S., Bandara, K., Burkert, A., Buschkamp, P., Carollo, C. M., Cresci, G., Davies, R., Eisenhauer, F., Hicks, E. K. S., Kurk, J., Lilly, S. J., Lutz, D., Mancini, C., Naab, T., Newman, S., Peng, Y., Renzini, A., Shapiro Griffin, K., Sternberg, A., Vergani, D., Wisnioski, E., Wuyts, E., and Zamorani, G. (2014). "The SINS/zC-SINF Survey of z ~2 Galaxy Kinematics: Evidence for Gravitational Quenching." , *785*(1), 75.

Genzel, R., Tacconi, L. J., Lutz, D., Saintonge, A., Berta, S., Magnelli, B., Combes, F., García-Burillo, S., Neri, R., Bolatto, A., Contini, T., Lilly, S., Boissier, J., Boone, F., Bouché, N., Bournaud, F., Burkert, A., Carollo, M., Colina, L., Cooper, M. C., Cox, P., Feruglio, C., Förster Schreiber, N. M., Freundlich, J., Gracia-Carpio, J., Juneau, S., Kovac, K., Lippa, M., Naab, T., Salome, P., Renzini, A., Sternberg, A., Walter, F., Weiner, B., Weiss, A., and Wuyts, S. (2015). "Combined CO and Dust Scaling Relations of Depletion Time and Molecular Gas Fractions with Cosmic Time, Specific Star-formation Rate, and Stellar Mass." , *800*(1), 20.

Glover, S. C. O., and Clark, P. C. (2016). "Is atomic carbon a good tracer of molecular gas in metal-poor galaxies?" , *456*(4), 3596–3609.

Guilloteau, S., and Lucas, R. (2000). "Imaging at the IRAM Plateau de Bure Interferometer." In J. G. Mangum, and S. J. E. Radford (Eds.), *Imaging at Radio through Submillimeter Wavelengths*, *Astronomical Society of the Pacific Conference Series*, vol. 217, 299.

Harrington, K. (2020). "Characterizing the Mean Molecular ISM Properties of Turbulent Starbursts at z = 1-3 via rest-frame far-IR/mm spectroscopy." In *American Astronomical Society Meeting Abstracts #235*, *American Astronomical Society Meeting Abstracts*, vol. 235, 407.03.

Hollenbach, D. J., and Tielens, A. G. G. M. (1997). "Dense Photodissociation Regions (PDRs)." , *35*, 179–216.

Hollenbach, D. J., and Tielens, A. G. G. M. (1999). "Photodissociation regions in the interstellar medium of galaxies." *Reviews of Modern Physics*, *71*(1), 173–230.

Ikeda, M., Oka, T., Tatematsu, K., Sekimoto, Y., and Yamamoto, S. (2002). "The Distribution of Atomic Carbon in the Orion Giant Molecular Cloud 1." , *139*(2), 467–485.

Israel, F. P., Rosenberg, M. J. F., and van der Werf, P. (2015). "Neutral carbon and CO in 76 (U)LIRGs and starburst galaxy centers. A method to determine molecular gas properties in luminous galaxies." , *578*, A95.

Kamenetzky, J., Glenn, J., Rangwala, N., Maloney, P., Bradford, M., Wilson, C. D., Bendo, G. J., Baes, M., Boselli, A., Cooray, A., Isaak, K. G., Lebouteiller, V., Madden, S., Panuzzo, P., Schirm, M. R. P., Spinoglio, L., and Wu, R. (2012). "Herschel-SPIRE Imaging Spectroscopy of Molecular Gas in M82." , *753*(1), 70.

Kulesa, C. A., Hungerford, A. L., Walker, C. K., Zhang, X., and Lane, A. P. (2005). "Large-Scale CO and [C I] Emission in the ρ Ophiuchi Molecular Cloud." , *625*(1), 194–209.

Lee, M. M., Tanaka, I., Iono, D., Kawabe, R., Kodama, T., Kohno, K., Saito, T., and Tamura, Y. (2021). "Revisited Cold Gas Content with Atomic Carbon [C I] in z = 2.5 Protocluster Galaxies." , *909*(2), 181.

Lequeux, J. (2005). *The Interstellar Medium*.

Leroy, A. K., Walter, F., Brinks, E., Bigiel, F., de Blok, W. J. G., Madore, B., and Thornley, M. D. (2008). "The Star Formation Efficiency in Nearby Galaxies: Measuring Where Gas Forms Stars Effectively." , *136*(6), 2782–2845.

Madau, P., and Dickinson, M. (2014). "Cosmic Star-Formation History." , *52*, 415–486.

Mashian, N., Sturm, E., Sternberg, A., Janssen, A., Hailey-Dunsheath, S., Fischer, J., Contursi, A., González-Alfonso, E., Graciá-Carpio, J., Poglitsch, A., Veilleux, S., Davies, R., Genzel, R., Lutz, D., Tacconi, L., Verma, A., Weiß, A., Polisensky, E., and Nikola, T. (2015). "High-J CO Sleds in Nearby Infrared Bright Galaxies Observed By Herschel/PACS." , *802*(2), 81.

Muzzin, A., Marchesini, D., Stefanon, M., Franx, M., McCracken, H. J., Milvang-Jensen, B., Dunlop, J. S., Fynbo, J. P. U., Brammer, G., Labbé, I., and van Dokkum, P. G. (2013). "The Evolution of the Stellar Mass Functions of Star-forming and Quiescent Galaxies to z = 4 from the COSMOS/UltraVISTA Survey." , *777*(1), 18.

Narayanan, D., and Krumholz, M. R. (2014). "A theory for the excitation of CO in star-forming galaxies." , *442*(2), 1411–1428.

Offner, S. S. R., Bisbas, T. G., Bell, T. A., and Viti, S. (2014). "An alternative accurate tracer of molecular clouds: the 'XCi-factor'." , *440*, L81–L85.

Okada, Y., Güsten, R., Requena-Torres, M. A., Röllig, M., Stutzki, J., Graf, U. U., and Hughes, A. (2019). "Velocity profiles of [C_{II}], [C_I], CO, and [O_I] and physical conditions in four star-forming regions in the Large Magellanic Cloud." , *621*, A62.

Planck Collaboration, Aghanim, N., Akrami, Y., Ashdown, M., Aumont, J., Baccigalupi, C., Ballardini, M., Banday, A. J., Barreiro, R. B., Bartolo, N., Basak, S., Battye, R., Benabed, K., Bernard, J. P., Bersanelli, M., Bielewicz, P., Bock, J. J., Bond, J. R., Borrill, J., Bouchet, F. R., Boulanger, F., Bucher, M., Burigana, C., Butler, R. C., Calabrese, E., Cardoso, J. F., Carron, J., Challinor, A., Chiang, H. C., Chluba, J., Colombo, L. P. L., Combet, C., Contreras, D., Crill, B. P., Cuttaia, F., de Bernardis, P., de Zotti, G., Delabrouille, J., Delouis, J. M., Di Valentino, E., Diego, J. M., Doré, O., Douspis, M., Ducout, A., Dupac, X., Dusini, S., Efstathiou, G., Elsner, F., Enßlin, T. A., Eriksen, H. K., Fantaye, Y., Farhang, M., Fergusson, J., Fernandez-Cobos, R., Finelli, F., Forastieri, F., Frailis, M., Fraisse, A. A., Franceschi, E., Frolov, A., Galeotta, S., Galli, S., Ganga, K., Génova-Santos, R. T., Gerbino, M., Ghosh, T., González-Nuevo, J., Górski, K. M., Gratton, S., Gruppuso, A., Gudmundsson, J. E., Hamann, J., Handley, W., Hansen, F. K., Herranz, D., Hildebrandt, S. R., Hivon, E., Huang, Z., Jaffe, A. H., Jones, W. C., Karakci, A., Keihänen, E., Keskitalo, R., Kiiveri, K., Kim, J., Kisner, T. S., Knox, L., Krachmalnicoff, N., Kunz, M., Kurki-Suonio, H., Lagache, G., Lamarre, J. M., Lasenby, A., Lattanzi, M., Lawrence, C. R., Le Jeune, M., Lemos, P., Lesgourgues, J., Levrier, F., Lewis, A., Liguori, M., Lilje, P. B., Lilley, M., Lindholm, V., López-Caniego, M., Lubin, P. M., Ma, Y. Z., Macías-Pérez, J. F., Maggio, G., Maino, D., Mandolesi, N., Mangilli, A., Marcos-Caballero, A., Maris, M., Martin, P. G., Martinelli, M., Martínez-González, E., Matarrese, S., Mauri, N., McEwen, J. D., Meinhold, P. R., Melchiorri, A., Mennella, A., Migliaccio, M., Millea, M., Mitra, S., Miville-Deschênes, M. A., Molinari, D., Montier, L., Morgante, G., Moss, A., Natoli, P., Nørgaard-Nielsen, H. U., Pagano, L., Paoletti, D., Partridge, B., Patanchon, G., Peiris, H. V., Perrotta, F., Pettorino, V., Piacentini, F., Polastri, L., Polenta, G., Puget, J. L., Rachen, J. P., Reinecke, M., Remazeilles, M., Renzi, A., Rocha, G., Rosset, C., Roudier, G., Rubiño-Martín, J. A., Ruiz-Granados, B., Salvati, L., Sandri, M., Savelainen, M., Scott, D., Shellard, E. P. S., Sirignano, C., Sirri, G., Spencer, L. D., Sunyaev, R., Suur-Uski, A. S., Tauber, J. A., Tavagnacco, D., Tenti, M., Toffolatti, L., Tomasi, M., Trombetti, T., Valenziano, L., Valiviita, J., Van Tent, B., Vibert, L., Vielva, P., Villa, F., Vittorio, N., Wandelt, B. D., Wehus, I. K., White, M., White, S. D. M., Zacchei, A., and Zonca, A. (2020). "Planck 2018 results. VI. Cosmological parameters." , *641*, A6.

Popping, G., Decarli, R., Man, A. W. S., Nelson, E. J., Béthermin, M., De Breuck, C., Mainieri, V., van Dokkum, P. G., Gullberg, B., van Kampen, E., Spaans, M., and Trager, S. C. (2017). "ALMA reveals starburst-like interstellar medium conditions in a compact star-forming galaxy at z 2 using [CI] and CO." , *602*, A11.

Requena-Torres, M. A., Israel, F. P., Okada, Y., Güsten, R., Stutzki, J., Risacher, C., Simon, R., and Zinnecker, H. (2016). "Carbon gas in SMC low-metallicity star-forming regions." , *589*, A28.

Rodighiero, G., Daddi, E., Baronchelli, I., Cimatti, A., Renzini, A., Aussel, H., Popesso, P., Lutz, D., Andreani, P., Berta, S., Cava, A., Elbaz, D., Feltre, A., Fontana, A., Förster Schreiber, N. M., Franceschini, A., Genzel, R., Grazian, A., Gruppioni, C., Ilbert, O., Le

Floch, E., Magdis, G., Magliocchetti, M., Magnelli, B., Maiolino, R., McCracken, H., Nordon, R., Poglitsch, A., Santini, P., Pozzi, F., Riguccini, L., Tacconi, L. J., Wuyts, S., and Zamorani, G. (2011). "The Lesser Role of Starbursts in Star Formation at z = 2." , *739*(2), L40.

Schreiber, C., Elbaz, D., Pannella, M., Ciesla, L., Wang, T., and Franco, M. (2018). "Dust temperature and mid-to-total infrared color distributions for star-forming galaxies at 0 ¡ z ¡ 4." , *609*, A30.

Scoville, N., Sheth, K., Aussel, H., Vanden Bout, P., Capak, P., Bongiorno, A., Casey, C. M., Murchikova, L., Koda, J., Álvarez-Márquez, J., Lee, N., Laigle, C., McCracken, H. J., Ilbert, O., Pope, A., Sanders, D., Chu, J., Toft, S., Ivison, R. J., and Manohar, S. (2016). "Erratum: "ISM Masses and the Star Formation Law at Z = 1 to 6 Alma Observations of Dust Continuum in 145 Galaxies in the Cosmos Survey Field" ¡A href="/abs/2016ApJ...820...83S"¿(2016, ApJ, 820, 83)¡/A¿." , *824*(1), 63.

Shimajiri, Y., Sakai, T., Tsukagoshi, T., Kitamura, Y., Momose, M., Saito, M., Oshima, T., Kohno, K., and Kawabe, R. (2013). "Extensive [C I] Mapping toward the Orion-A Giant Molecular Cloud." , *774*(2), L20.

Solomon, P. M., and Vanden Bout, P. A. (2005). "Molecular Gas at High Redshift." , *43*(1), 677–725.

Stutzki, J., Graf, U. U., Haas, S., Honingh, C. E., Hottgenroth, D., Jacobs, K., Schieder, R., Simon, R., Staguhn, J., Winnewisser, G., Martin, R. N., Peters, W. L., and McMullin, J. P. (1997). "Atomic Carbon in M82: Physical Conditions Derived from Simultaneous Observations of the [C I] Fine-Structure Submillimeter-Wave Transitions." , *477*(1), L33–L36.

Tacconi, L. J., Genzel, R., Saintonge, A., Combes, F., García-Burillo, S., Neri, R., Bolatto, A., Contini, T., Förster Schreiber, N. M., Lilly, S., Lutz, D., Wuyts, S., Accurso, G., Boissier, J., Boone, F., Bouché, N., Bournaud, F., Burkert, A., Carollo, M., Cooper, M., Cox, P., Feruglio, C., Freundlich, J., Herrera-Camus, R., Juneau, S., Lippa, M., Naab, T., Renzini, A., Salome, P., Sternberg, A., Tadaki, K., Übler, H., Walter, F., Weiner, B., and Weiss, A. (2018). "PHIBSS: Unified Scaling Relations of Gas Depletion Time and Molecular Gas Fractions." , *853*(2), 179.

Tacconi, L. J., Neri, R., Genzel, R., Combes, F., Bolatto, A., Cooper, M. C., Wuyts, S., Bournaud, F., Burkert, A., Comerford, J., Cox, P., Davis, M., Förster Schreiber, N. M., García-Burillo, S., Gracia-Carpio, J., Lutz, D., Naab, T., Newman, S., Omont, A., Saintonge, A., Shapiro Griffin, K., Shapley, A., Sternberg, A., and Weiner, B. (2013). "Phibss: Molecular Gas Content and Scaling Relations in z ~1-3 Massive, Main-sequence Star-forming Galaxies." , *768*(1), 74.

Talia, M., Pozzi, F., Vallini, L., Cimatti, A., Cassata, P., Fraternali, F., Brusa, M., Daddi, E., Delvecchio, I., Ibar, E., Liuzzo, E., Vignali, C., Massardi, M., Zamorani, G., Gruppioni, C., Renzini, A., Mignoli, M., Pozzetti, L., and Rodighiero, G. (2018). "ALMA view of a massive spheroid progenitor: a compact rotating core of molecular gas in an AGN host at z = 2.226." , *476*(3), 3956–3963.

Tielens, A. G. G. M. (2005). *The Physics and Chemistry of the Interstellar Medium*.

Valentino, F., Daddi, E., Puglisi, A., Magdis, G. E., Liu, D., Kokorev, V., Cortzen, I., Madden, S., Aravena, M., Gómez-Guijarro, C., Lee, M. Y., Le Floc'h, E., Gao, Y., Gobat, R., Bournaud, F., Dannerbauer, H., Jin, S., Dickinson, M. E., Kartaltepe, J., and Sanders, D. (2020a). "CO emission in distant galaxies on and above the main sequence." , *641*, A155.

Valentino, F., Magdis, G. E., Daddi, E., Liu, D., Aravena, M., Bournaud, F., Cibinel, A., Cormier, D., Dickinson, M. E., Gao, Y., Jin, S., Juneau, S., Kartaltepe, J., Lee, M.-Y., Madden, S. C., Puglisi, A., Sanders, D., and Silverman, J. (2018). "A Survey of Atomic Carbon [C I] in High-redshift Main-sequence Galaxies." , *869*(1), 27.

Valentino, F., Magdis, G. E., Daddi, E., Liu, D., Aravena, M., Bournaud, F., Cortzen, I., Gao, Y., Jin, S., Juneau, S., Kartaltepe, J. S., Kokorev, V., Lee, M.-Y., Madden, S. C., Narayanan, D., Popping, G., and Puglisi, A. (2020b). "The Properties of the Interstellar Medium of Galaxies across Time as Traced by the Neutral Atomic Carbon [C I]." , *890*(1), 24.

van der Tak, F. F. S., Black, J. H., Schöier, F. L., Jansen, D. J., and van Dishoeck, E. F. (2007). "A computer program for fast non-LTE analysis of interstellar line spectra. With diagnostic plots to interpret observed line intensity ratios." , *468*(2), 627–635.

van der Werf, P. P., Isaak, K. G., Meijerink, R., Spaans, M., Rykala, A., Fulton, T., Loenen, A. F., Walter, F., Weiß, A., Armus, L., Fischer, J., Israel, F. P., Harris, A. I., Veilleux, S., Henkel, C., Savini, G., Lord, S., Smith, H. A., González-Alfonso, E., Naylor, D., Aalto, S., Charmandaris, V., Dasyra, K. M., Evans, A., Gao, Y., Greve, T. R., Güsten, R., Kramer, C., Martín-Pintado, J., Mazzarella, J., Papadopoulos, P. P., Sanders, D. B., Spinoglio, L., Stacey, G., Vlahakis, C., Wiedner, M. C., and Xilouris, E. M. (2010). "Black hole accretion and star formation as drivers of gas excitation and chemistry in Markarian 231." , *518*, L42.

Walter, F., Weiß, A., Downes, D., Decarli, R., and Henkel, C. (2011). "A Survey of Atomic Carbon at High Redshift." , *730*(1), 18.

Weiß, A., Downes, D., Henkel, C., and Walter, F. (2005). "Atomic carbon at redshift ∼2.5." , *429*, L25–L28.

Weiß, A., Henkel, C., Downes, D., and Walter, F. (2003). "Gas and dust in the Cloverleaf quasar at redshift 2.5." , *409*, L41–L45.

Whitaker, K. E., van Dokkum, P. G., Brammer, G., and Franx, M. (2012). "The Star Formation Mass Sequence Out to z = 2.5." , *754*(2), L29.

Yang, C., Omont, A., Beelen, A., Gao, Y., van der Werf, P., Gavazzi, R., Zhang, Z. Y., Ivison, R., Lehnert, M., Liu, D., Oteo, I., González-Alfonso, E., Dannerbauer, H., Cox, P., Krips, M., Neri, R., Riechers, D., Baker, A. J., Michałowski, M. J., Cooray, A., and Smail, I. (2017). "Molecular gas in the Herschel-selected strongly lensed submillimeter galaxies at z 2-4 as probed by multi-J CO lines." , *608*, A144.